Modeling Fluoride Adsorption on Cerium-Loaded Cellulose Bead—Response Surface Methodology, Equilibrium, and Kinetic Studies

Mitali Sarkar · Dhiman Santra

Abstract A novel cerium-loaded cellulose nanocomposite bead (CCNB) is synthesized and tested for fluoride adsorption. The optimization of the process under the cooperative influence of different experimental variables was made employing response surface methodology (RSM). It is found from fractional factorial design (FFD) that among the different experimental variables, only adsorbent dose, temperature, and pH are significant. At the optimum condition (adsorbent dose 1 g L^{-1}, temperature 313 K, pH 3.0), a maximum fluoride adsorption of 94 % was observed for an initial fluoride concentration of 2.5 mg L^{-1}. A quadratic polynomial model equation based on central composite design (CCD) was built to predict the extent of adsorption. The result of the analysis of variance (ANOVA) shows high coefficients of determination (correlation coefficient; $R^2=0.9772$, adjusted $R^2=0.9545$, and adequate precision=18.1045) and low probability value (Prob > F, 0.001) which signifies the validity of the model. The equilibrium adsorption data conformed to the Tempkin isotherm, having higher R^2 and lower SE value, among the Langmuir, Freundlich, and Tempkin equations at different temperatures. The adsorption data was found to fit well the second-order rate equation with film diffusion governing the overall rate. The activation energy value was calculated to be 16.74 kJ mol^{-1}. Fluoride can be eluted from fluoride-loaded CCNB using alkali. CCNB can be reused at least for five successive operations.

1 Introduction

The elevated level of fluoride in ground water around the globe as a consequence of minerals leaching is reported (Chand 1999). In India, 17 states (Jagtap et al. 2012) at present are worst affected with fluorosis, the fluoride-related health ailment (Teutli-Sequeira et al. 2012). Adsorptive removal by far is the most popular technique considering the operational simplicity, applicability in wide range of solution condition, and repetitive use of adsorbent via recycling (Alagumuthu and Ranjan 2010). Generation of sludge during precipitation (Larsen and Pearce 2002) and coagulation (Hu et al. 2005), tedious preparation of suitable ion exchange resin (Castel et al. 2000; Veressinina et al. 2001), and strict control of operational condition in membrane technique (Sehn 2008) are some of the major problems encountered during removal of contaminants in water. A wide variety of adsorbents such as natural (Sarkar et al. 2006a), synthetic (Alagumuthu and Ranjan 2010; Camacho et al. 2010; Viswanathan et al. 2009), and

M. Sarkar (✉) · D. Santra
Department of Chemistry, University of Kalyani,
Kalyani 741 235, India
e-mail: mitali_ku@yahoo.com

M. Sarkar
e-mail: msarkar@klyuniv.ac.in

waste material (Sarkar et al. 2008; Medellin-Castillo et al. 2007) has been reported for fluoride removal.

However, biopolymer, due to its degradable character and easy availability in nature, becomes a popular choice for preparation of new generation adsorbents. Cellulose being the most abundant one, on modification with transition metal, e.g., cerium, is used for fluoride removal. The bead form of the adsorbent in the present case facilitates its mechanical separation from solution.

The surface characterization of the adsorbent was made by field emission scanning electron microscopy (FESEM) analysis. The general properties were evaluated from density, porosity, and swelling character of the bead. Fluoride interaction with the synthesized bead was evaluated by energy dispersive spectroscopy (EDS), Fourier transform infrared spectroscopy (FTIR), and electron paramagnetic resonance (EPR) study. The optimum adsorption condition for experimental variables such as initial fluoride concentration, adsorbent dose, pH, agitation time, and temperature was evaluated. Response surface methodology, one of the most popular design tools, is used to design parametric condition and to predict adsorption extent through some quadratic model developed. The validity of the model was tested through the analysis of variance (ANOVA). The experimental equilibrium data was tested for the Langmuir, Freundlich, and Tempkin equation, and the corresponding isotherm constants at three different temperatures were evaluated. The Tempkin isotherm is shown to be suited most in the present case of adsorption. The adsorption kinetics was established by comparing first- and second-order kinetic models. The transport and diffusion phenomena were elucidated to find out the rate-limiting step. The activation energy was determined. Elution of fluoride was found effective with 10^{-2} N NaOH. Adsorption–elution operations for five successive times can be performed with cerium-loaded cellulose nanocomposite bead (CCNB).

2 Materials and Methods

2.1 Materials

All the chemicals and solvents used were of analytical grade (Merck, India). The cellulose power used was procured from Loba Chemie, Mumbai, India

2.2 Preparation of CCNB

Cellulose nanocomposite bead was prepared following the method described elsewhere (Wang et al. 2007). Alkaline cellulose was esterified by treatment with carbon disulfide, stirred, and aged for 72 h at room temperature. The viscose solution thus obtained was purged drop by drop into de-aerated methanol through a needle. A faint red-colored beads initially formed were filtered and immediately washed several times with double distilled water. The cellulose nanobead (CB), appeared as snow white, was stored under de-ionized water.

For incorporation of cerium, cerium ammonium nitrate solution (0.1 M) at pH 1.6 was added to CB and agitated at room temperature for 2 h. A faint orange yellow-colored cerium-loaded cellulose nanocomposite bead (CCNB) was formed, washed with distilled water, and stored under de-ionized water.

2.3 Characterization of CCNB

The element composition as well as the surface structure of CCNB was revealed from FESEM, EDS, FTIR, and electron paramagnetic resonance study (EPS).

2.4 Batch Sorption Study

Fluoride adsorption using CCNB was performed in batch mode in a 100-mL stoppered conical flask (Teflon). Twenty-five-milliliter solution of known concentration (1–10 mg L^{-1}) was shaken with 1.0 g of CCNB at a constant shaking rate of 120 spm in a temperature-controlled shaker until the equilibrium is attained. The initial solution pH was adjusted using 0.1 M HCl/NaOH. The experiment was performed at three different temperatures ranging from 293 to 323 K. Fluoride concentration in solution was determined potentiometrically using fluoride ion-sensitive electrode (9609BNWP) in an Orion ion meter (VSTAR52). The percent adsorption was calculated from the following equation:

$$\text{Percent adsorption}(\%) = (C_0 - C_e).100/C_0 \qquad (1)$$

where C_0 and C_e are the initial and equilibrium fluoride concentration (mg L^{-1}), respectively, in solution.

Desorption study was carried out by aqueous NaOH solution (10^{-2} N) for fluoride.

2.5 Design and Optimization of Adsorption Considering Competitive and Cooperative Effect of Multiple Variables

The conventional and classical adsorption experiment is generally designed to find out influence of each experimental variable individually keeping others at some unspecified constant level. Thus, the optimization of process operation needs a large number of experiments. More importantly, this could not reflect the true situation of multiparameter effect, i.e., the combined influence of all the parameters involved (Behbahani et al. 2011). Design-Expert 8 software was employed here to execute the statistical optimization through response surface methodology (RSM) (Montgomery 2009). The nature and extent of interaction of process parameters, viz. pH, fluoride concentration (mg L^{-1}), adsorbent dosage (g L^{-1}), temperature (K), and time (min), were evaluated following fractional factorial design and central composite design.

2.5.1 Identification of Significant Variables from Fractional Factorial Design

Fractional factorial design (FFD), as the first step of RSM, was employed taking into account all possible combinations of all the variables across all the levels. This exploits the sparsity-of-effects principle and suitably selects the most significant variables among the studied variables. The levels of a variable are commonly coded as +1 (higher) and −1 (lower) and consider an alias structure from a full factorial experiment.

2.5.2 Optimization of Significant Variables by Central Composite Design

The central composite design (CCD) was applied to develop an empirical quadratic model for prediction of response and subsequently to estimate the model validity. Generally, CCD consists of factorial runs, axial runs, and center runs (six replicates) (Sereshti et al. 2009). Rotatable, orthogonal central composite design is employed to determine the optimal conditions for the critical factors.

The experimental sequence is randomized in order to minimize the effects of any uncontrollable variable. The response predicted (Y, the percent adsorption) is correlated with input process variables using a polynomial equation and is given by Eq. 2

$$Y = \beta_o + \sum_{i=1}^{k} \beta_i x_i + \sum_{i=1}^{k} \beta_{ii} x_i^2 \qquad (2)$$
$$+ \sum_{i=1}^{k-1} \sum_{j=2}^{k} \beta_{ij} x_i x_j + \varepsilon$$

Here, x_i^2, x_j^2,…, x_k^2 denotes the square effects, $x_i x_j$, $x_i x_k$, and $x_j x_k$, the interaction effects, β_0 is the constant intercept term, β_i (i=1, 2,…, k) is the coefficient of linear effect, β_{ii} (i=1, 2, . . ., k) is the coefficient of squared effect, β_{ij} (i=1, 2,…, k; j=1, 2,…, k) is the coefficient of interaction effect, and ε is a random error (Aksu and Gonen 2006; Goksungur et al. 2005). The validity, significance, and adequacy of the above polynomial are estimated from ANOVA, particularly by the value of correlation coefficient (R^2), Fisher variation ratio (F value), probability (Prob > F), and adequate precision (Montgomery 2009; Sarkar and Majumdar 2011).

3 Results and Discussion

3.1 Characterization of CCNB

3.1.1 General Characterization

The particle characterization of the synthesized bead was made and the parameters are given in Table 1.

3.1.2 FESEM, EDS, and EPS Analysis

The surface structure of CCNB was revealed from FESEM analysis which indicates spherical nature of the bead with an average size in the range 28 to 61 nm. The EDS shows peaks corresponding to the presence of "C," "O," and cerium ("Ce") in the CCNB. The presence of fluoride in the bead

Table 1 Particle characterization of CCNB

Sl. no	Parameter	Value
1	Bulk density (g cm^{-3})	0.902
2	Material density (g cm^{-3})	0.410
3	Water content (%)	95.120
4	Degree of swelling	22
5	Porosity (%)	89

after fluoride adsorption is evident from the appearance of a new peak. The EPS study conducted at room temperature (303 K) and lower temperature (77 K) shows similar signals having characteristics g values attributed to $g_e=2.03$, $g\perp=1.98$, $g_\Pi=1.93$ ($g_e>g\perp>g_\Pi$), (Abi-aad et al. 1993) corresponding to Ce^{3+}. The FTIR spectral analysis of CCNB showing the characteristic bands of cellulose moiety with different linkages (Jagtap et al. 2009; Li et al. 2010; Rocha and Muccillo 2003) is presented in Table 2.

Fluoride-loaded CCNB shows similar IR bands. In addition, prominent shifting of the band position from 535 to 499 cm^{-1} with significant intensity change indicates the interaction of fluoride with cerium (Santra et al. 2014).

3.2 Stability of CCNB

The stability of the synthesized bead was tested for heat and acid/alkali treatment. The bead was found to remain unchanged in particle and material character when heated at least up to 323 K. This can be supported from the unchanged physical parameters as well as the IR spectra of the bead. The bead was resistant to acid treatment. In an acidic environment, CCNB retains its shape, size, and composition and no cerium leaching was observed. However, in alkaline condition (pH >12), the bead undergoes slow and gradual degradation. Thus, stability and high adsorption capacity of CCNB make it a quite promising biosorbent for fluoride removal (Yadav et al. 2013).

Table 2 FTIR spectral analysis of CCNB

Position (cm^{-1})	Origin
3402	O–H stretching vibration
2918	C–H stretching vibration
1642	Molecular water bending
1424	C–O–H and C–C–H deformations
1375–1317	C–H flexure vibration (symmetric)
1161, 1060	C–O stretching vibration
898	C–H bending vibration from the β-anomeric link of cellulose
769	C–C stretching vibration
535	Ce–O linkage

3.3 Optimization of Fluoride Adsorption Using RSM

3.3.1 Fractional Factorial Design

FFD was employed primarily to identify and select/eliminate the variables in terms of their influence on response (Brereton 2003). In the present case, a half-fractional factorial design (2^{5-1}) with 16 experiments (divided into two blocks, each with eight experiments and run in a random manner) was executed. The most important effects and interactions of the primary variables [pH, fluoride concentration (mg L^{-1}), adsorbent dosage (g L^{-1}), temperature (K), and time (min)] on the response (adsorption %) are examined from ANOVA through F value and P value (Prob > F) (Table 3). The model F value of 8.24 implies that the model is significant. There is only a 0.36 % chance that the F value could occur due to noise. The P value <0.0001 obtained (Prob > F less than 0.0500) indicates that the model term is significant.

The results of ANOVA reveal that pH, fluoride concentration, adsorbent dosage, and temperature are the most significant, i.e., critical parameters for multivariate optimization through CCD in the next step.

3.3.2 Central Composite Design

The preliminary levels of the factorial (+ and −), the star (+ and −), and the center points of the experimental variables are selected to develop a quadratic model. The total number of experimental data points (E.D.P) required to build the suitable design was calculated (Sarkar and Majumdar 2011) from Eq. 3,

$$E.D.P = 2^k(\text{factorial}) + 2k(\text{axial}) + 6(\text{center}) \qquad (3)$$

where k is the number of variables (k=3 and E.D.P=20, in this case).

Experiments corresponding to center points are usually repeated to get a good estimate of experimental error (pure error). As each adsorption experiment is conducted using some fixed fluoride concentration, CCD is operated with three significant variables only, i.e., pH, adsorbent dosage (g L^{-1}), and temperature (K). The corresponding coded values taken are A, B, and C, respectively. A model equation is built to correlate percent adsorption of fluoride and cooperative effects of significant variables at the optimized condition. The proposed quadratic equation is consisted of three

Table 3 ANOVA for a (2^{5-1}) fractional factorial design

Parameter	Sum of square	DOF[a]	Mean square	F value[b]	P value,[c] (Prob > F)
Model	1089.5	5	217.9	8.239916	0.0036*
pH	361	1	361	13.65126	0.005*
Fluoride concentration	156.25	1	156.25	5.908613	0.0379*
Adsorbent dose	156.25	1	156.25	5.908613	0.0379*
Temperature	400	1	400	15.12605	0.0037*
Time	16	1	16	0.605042	0.4566**
Residual	238	9	26.4444		
Cor total	1329.75	15			

F value when the null hypothesis is true

*$p<0.05$, significant;.**$p>0.05$, not significant

[a] Degree of freedom

[b] Test for comparing model with residual (error) variance

[c] Probability of finding

principal effects, three two-factor interaction effects, and three curvature effects. The adsorption percent (Y) of fluoride in terms of the coded factors is described by Eq. 4 as follows.

$$\text{Percent adsorption} = 91.0408 - 3.4012A + 3.0487B - 3.4980C$$
$$- 0.25AB - 4.75AC + 5.5BC - 16.0090A^2$$
$$- 13.3225B^2 - 13.8528C^2 \qquad (4)$$

The magnitude of the coefficient denotes the intensity while the sign indicates the nature of influence of the variable on the response.

The empirical relationship between percent adsorption and the process variables in terms of actual factors can be expressed by Eq. 5:

$$\text{Percent adsorption} = -133340.80 + 96.90 \text{ pH} - 230.87 \text{ dose}$$
$$+ 85.98 \text{ temp} - 0.25 \text{ pH. dose}$$
$$- 0.23 \text{ pH. temp} + 1.10 \text{ dose. temp}$$
$$- 4.00 \text{ pH}^2 - 53.29 \text{ dose}^2 - 0.13 \text{ temp}^2$$
$$(5)$$

The statistical significance of the proposed model was evaluated from ANOVA and is presented in Table 4. The quality of the model is tested through F and P values. The F value of 42.96 implies that the model is significant and there is only a 0.01 % chance that the F value could occur due to noise. The low probability value, viz. 0.001, indicates that the model is significant. As a Prob > F value less than 0.0500 indicates the terms significant and that greater than 0.1000 not significant, in this case, A, B, C, AC, BC, A^2, B^2, and C^2 are significant. Further, the value of adequate precision (>4) and closeness in the values of R-squared (R^2), adjusted R-squared (R^2_{Adj}), and predicted R-squared (R^2_{Pred}) adequately supports the proposed

model. The small deviation may be due to some nonlinear influence of the variables on the response.

3.4 Adsorption Isotherm

Adsorption is an equilibrium operation that governs the solute retention at solid–solution interface at constant temperature (Allen et al. 2004). The equilibrium is established when the solute has been contacted with the adsorbent for a sufficient time and the concentration of solute in the bulk solution is in a dynamic balance with the interface concentration (Ghiaci et al. 2004). The mathematical correlation between the amount of solute retained on adsorbent over the concentration of solute in solution is known as adsorption isotherm. The applicability of a particular isotherm such as Langmuir, Freundlich, and Tempkin, commonly used for operational design and applicable practice, is tested for the present solute–adsorbent system.

Langmuir adsorption isotherm (Langmuir 1916) assumes that:

i.   Adsorption is monolayer in nature,
ii. Adsorption can only occur at a finite number of definite localized sites that are identical and equivalent, and
iii. There is no lateral interaction and steric hindrance between the adsorbed molecules, even on adjacent sites.

Langmuir isotherm in its linear form is represented as

$$C_e/q_e = 1/Q_l b_l + C_e/Q_l \qquad (6)$$

where C_e (mg L^{-1}) and q_e (mg g^{-1}) represent concentration of solute in solution and amount of solute

Table 4 ANOVA for the response surface quadratic model

Parameter	Sum of square	DOF[a]	Mean square	F value[b]	P value,[c] (Prob > F)
Model	8548.583	9	949.8426	42.96215	<0.0001*
A—pH	121.9366	1	121.9366	5.515292	0.0434*
B—adsorbent dose	126.9359	1	126.9359	5.741412	0.0402*
C—temperature	167.1114	1	167.1114	7.558586	0.0225*
AB	0.5	1	0.5	0.022615	0.8838**
AC	180.5	1	180.5	8.164161	0.0189*
BC	242	1	242	10.94586	0.0091*
A^2	2263.856	1	2263.856	102.396	<0.0001*
B^2	2577.256	1	2577.256	116.5714	<0.0001*
C^2	2786.526	1	2786.526	126.0368	<0.0001*
Residual	198.9794	9	22.10882		
Lack of fit	194.7919	5	38.95838	37.21398	0.0019*
Pure error	4.1875	4	1.046875		
Cor total	8810.638	19			

$R^2 = 0.9772$, $R^2_{Adj} = 0.9545$, $R^2_{Pred} = 0.8129$, adequate precision=18.1045. F value when the null hypothesis is true

*$p < 0.05$, significant; **$p > 0.05$, not significant

[a] Degree of freedom

[b] Test for comparing model with residual (error) variance

[c] Probability of finding

adsorbed at equilibrium, respectively, and Q_l (mg g^{-1}) and b_l (L mg^{-1}) are the Langmuir isotherm constants related to adsorption capacity and energy, respectively.

A plot of C_e/q_e against C_e at constant temperature yields straight line. Q_l and b_l corresponding to three different temperatures are obtained from the slope and the intercept, respectively. It is found that the value of both Q_l and b_l increases with increase in temperature.

The Freundlich isotherm model (Freundlich 1906) assumes that:

i.   It is associated with heterogeneous sites,
ii. The stronger binding sites are occupied first, and
iii. The adsorption energy is exponentially decreased upon the completion of adsorption process.

The linear form of Freundlich isotherm is represented as

$$\ln q_e = \ln C_e + (1/n_f)\ln C_e \qquad (7)$$

where K_f (L g^{-1}) and $1/n_f$ signify the capacity and the intensity, respectively, with C_e and q_e having usual significance. A plot of $\ln q_e$ against $\ln C_e$ should yield straight line with slope $1/n_f$ and intercept $\ln K_f$,

respectively. K_f value is found to be increased with temperature and intensity value <1 indicates the favorable situation.

Tempkin isotherm (Temkin and Pyzhev 1940) assumes that:

i. Heat of adsorption would decrease linearly rather than logarithmic with coverage and
ii. A uniform distribution of binding energies occurs.

The isotherm is represented as

$$q_e = (RT/b_{tm})\ln k_{tm} + (RT/b_{tm})\ln C_e \qquad (8)$$

where k_{tm} (L mg^{-1}) represents the isotherm constant and b_{tm} (kJ mol^{-1}) represents the heat of adsorption. A straight line with slope of RT/b_{tm} and intercept of $(RT/b_{tm})\ln k_{tm}$ is obtained from the plot of q_e against $\ln C_e$. It is found that while k_{tm} increases with temperature, no definite trend is observed for b_{tm}.

In order to test the adherence of experimental data to a particular isotherm model, the statistical parameters, viz. regression coefficient (R^2) and standard error (SE), were estimated for each isotherm (Table 5). The higher value of R^2 suggests the quality of good data fit. In a

Table 5 Evaluation of isotherm constants

Isotherm					
Langmuir	Temp (K)	$Q_1.10^2$ (mg g^{-1})	b_1, 10^2 (L mg^{-1})	R^2	SE
	293	39.01	47.91	0.993	0.832
	303	39.88	86.50	0.975	1.531
	313	41.60	101.20	0.986	0.948
Freundlich	Temp (K)	$K_f.10^2$ (g L^{-1})	$1/n_f$	R^2	SE
	293	12.51	0.46	0.982	0.078
	303	16.72	0.39	0.954	0.126
	313	18.30	0.41	0.961	0.119
Tempkin	Temp (K)	k_{tm} (L mg^{-1})	b_{tm} (kJ mol^{-1})	R^2	SE
	293	5.06	29.71	0.995	0.006
	303	10.85	32.29	0.969	0.019
	313	12.33	31.79	0.985	0.014

situation of similar values of R^2, the guiding parameter is the SE value (Sarici-Özdemir and Önal 2014). The lower the value of SE, the more acceptable is the isotherm model. It is found that R^2 value for the Freundlich isotherm is lower than that for both the Langmuir and Tempkin isotherm. The Langmuir and Tempkin possess comparable R^2 value. Since the SE value for the Tempkin isotherm is much lower than that for the Langmuir, it is said that Tempkin isotherm is most applicable for the present case of fluoride–CCNB adsorption. Moreover, the experimental data is compared with the model data from each isotherm, and the nature of experimental isotherm was assessed through fitting on each theoretical isotherm model (Fig. 1).
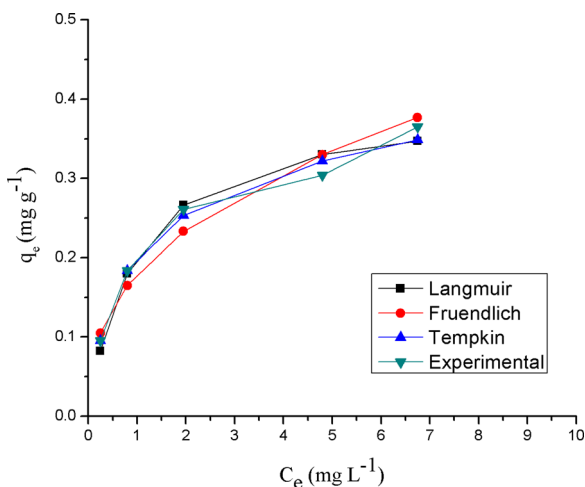
Fig. 1 Isotherm curve fitting plot

The isotherm constants for different isotherms together with the R^2 and SE values for different temperatures are presented in Table 5. The feasibility criteria of the adsorption process can be judged from the values of separation factor sf, defined (Weber and Chakravorti 1974) as,

$$\mathrm{sf} = 1/(1 + C_0 b_1) \tag{9}$$

From the value of sf evaluated, the nature of adsorption may be designated as favorable ($0<\mathrm{sf}<1$), linear ($\mathrm{sf}=1$), unfavorable ($\mathrm{sf}>1$), or irreversible ($\mathrm{sf}=0$). In the present situation, the sf values are found in between 0 and 1 and hence the adsorption of fluoride on CCNB is favorable. The feasibility criterion of present adsorption with varying concentrations at different temperature is illustrated in Fig. 2.

3.5 Adsorption Kinetics

3.5.1 Adsorption Rate Parameter

Adsorption kinetics is an important characteristic regarding the determination of the adsorption process efficiency. The adsorption of a solute on a solid from aqueous solution usually follows a complex kinetics. In an aim to understand the kinetics of the process, the data was fitted to different rate equations. A general rate expression takes the form

$$\mathrm{d}q/\mathrm{d}t = K_n(q_e - q_t)^n \tag{10}$$
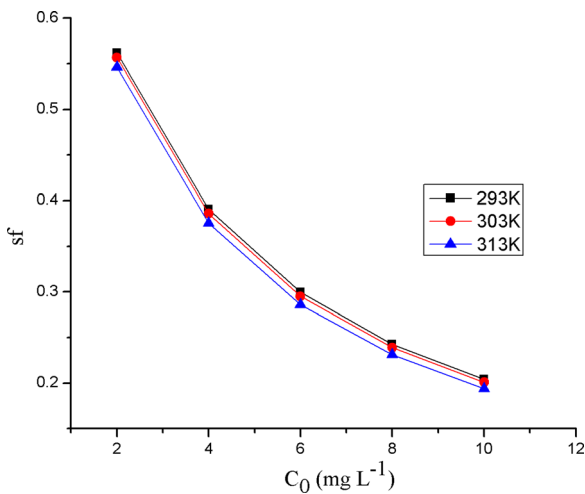
Fig. 2 Separation factor plot

where q_e and q_t are the amount of fluoride on CCNB (mg g^{-1}) at equilibrium and time t, respectively. K_n represents the rate constant corresponding to the order of the interaction.

The kinetics of fluoride adsorption on CCNB was tested for the pseudo-first-order and second-order kinetic model. The integrated pseudo-first-order rate equation (Chiou and Li 2003) is represented as

$$\ln(q_e - q_t) = \ln q_e - k_1 t \tag{11}$$

A plot of $\ln(q_e - q_t)$ vs. t at each temperature yields a straight line (Fig. 3a). The first-order rate constant k_1 (min^{-1}) is evaluated from the slope.

The linear form of the second-order kinetic equation (Ho and McKay 1999) is expressed as

$$t/q_t = 1/k_2 q_e^2 + t/q_t \tag{12}$$

Here, the boundary condition is for $t=0$ to t, $q_t=0$ to q_t. k_2 is the second-order rate constant (g mg^{-1} min^{-1}) and is evaluated from the intercept of the straight line plot of t/q_t against t at each temperature (Fig. 3b).

The suitability of a particular kinetic model was judged from the goodness of data fit and R^2 (regression coefficient) value (Table 6). The second-order kinetic equation with higher R^2 value may describe well the fluoride–CCNB interaction in the present situation. It is found that as temperature increases, k_2 also increases.

For a solid–liquid adsorption process, the solute transfer may be described by boundary layer and pore diffusion phenomena. The extent of each one to the overall process can be estimated from the Weber and

Morris equation (Rengaraj et al. 2007) described in Eq. 13.

$$q_t = k_p t^{0.5} \tag{13}$$

where k_p is the rate constant (mg g^{-1} min$^{-0.5}$) for pore diffusion and is determined (Table 6) from the slope of the linear portion of the plot of q_t vs. $t^{0.5}$ (Fig. 3c). The initial curved portion of the plot describes the surface adsorption while the linear portion is indicative of pore diffusion. The intercept of the plot estimates the extent of boundary layer effect. The larger the intercept, the greater is the contribution of surface adsorption or boundary layer diffusion toward overall process. It is found that k_p value decreases while the intercept increases with temperature. It may be estimated that at higher temperature, increased surface diffusion results due to surface activation.

A plot of the logarithm of pore diffusion constant ($\ln k_p$) against inverse of temperature ($1/T$) (Fig. 3d) was made to estimate the effect of temperature on solute–adsorbent interaction and to evaluate the activation energy.

$$\ln k_p = \ln A - E/RT \tag{14}$$

where A is the pre-exponential factor, R is the universal gas constant, and T is the absolute temperature. The activation energy of pore diffusion is calculated to be 13.17 kJ mol^{-1}.

3.5.2 Mechanistic Pathway of Adsorption

Transport of solute from bulk solution to the adsorbent–water interface and diffusion of solute from interface to the adsorbent surface are the two main steps that proceed with different rates. The slowest step between the two determines the rate of overall adsorption process. The kinetics of bulk transport can be characterized by β, the mass transfer coefficient, and is represented by Eq. 15 (Mckay et al. 1981).
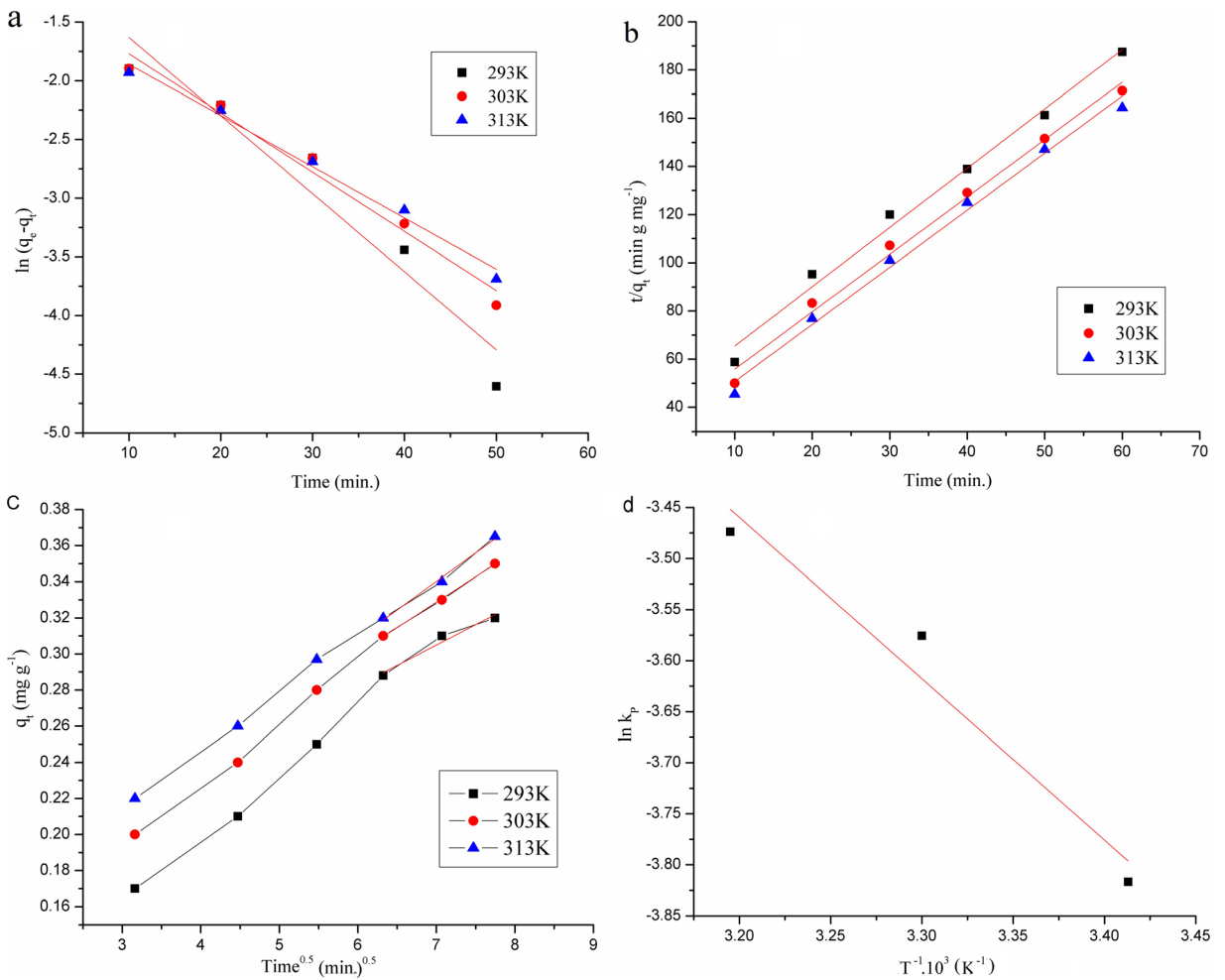
$$\ln P = \ln(M/N) - N\beta St/M \tag{15}$$

$$P = (C_t/C_0) - 1/(1 + mK_c) \tag{16}$$

$$M = mK_c \tag{17}$$

$$N = 1 + mK_c \tag{18}$$

Fig. 3 Plot of **a** pseudo-first-order kinetic equation, **b** second-order kinetic equation, **c** Weber Morris equation, and **d** Arrhenius equation

Table 6 Evaluation of kinetic parameters

Equation						
Pseudo 1st order	Temp (K)		k_1, 10^2 (min^{-1})			R^2
	293		6.62			0.936
	303		5.01			0.979
	313		4.31			0.989
2nd order	Temp (K)		k_2 .10^2 (g mg^{-1} min^{-1})			R^2
	293		14.77			0.990
	303		17.69			0.992
	313		20.72			0.992
Weber Morris/ Arrhenius	Temp (K)	k_p, 10^2 (gmg^{-1} min$^{-0.5}$)	Intercept 10^2	A	E (kJ mol^{-1})	R^2
	293	3.41	6.00	4.94	13.17	0.956
	303	3.30	9.41			
	313	3.12	12.10			

Here, C_0 is the initial fluoride concentration (mg L^{-1}) and C_t is that at time t, m is the mass (g) of CCNB, K_c is the equilibrium constant, and S is the specific surface area per unit volume (cm^{-1}) of particle-free solution.

A plot of ln$P$ vs. t (Fig. 4) gives the β value from the slope.

As the solute mobility increases with increased temperature, it is expected that β value should increase. The β value obtained from McKay equation plot also supports this. Further, as the solution is vigorously agitated, bulk transport of the solute cannot be the rate-limiting step. The observed increase in β value with increased temperature is expected probably due to the increase of solute mobility in solution.

Diffusion of solute through interfacial film boundary (surface diffusion) to the adsorbent surface constitutes the most vital step. At the same time, particle (pore and intraparticle) diffusion may also have some contribution. It is quite reasonable that film and particle diffusion occur at different rates, and the slowest one of the two is the rate-determining step governing the overall rate of adsorption.

The predominating role of a particular diffusion, among the three (film, pore, and intraparticle) actually governing the rate, can be evaluated by quantitative treatment of experimental data (Boyd et al. 1947). As intraparticle diffusion is generally very rapid, it rarely represents the rate-limiting step (Crank 1956). So, either film or pore diffusion should govern the process.

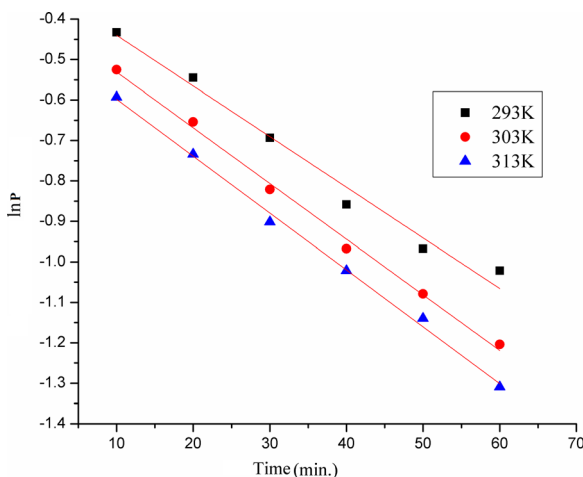Assuming all the nanoparticles of CCNB are uniform in shape and spherical in nature, particle diffusion can be

Fig. 4 McKay equation plot at different temperatures
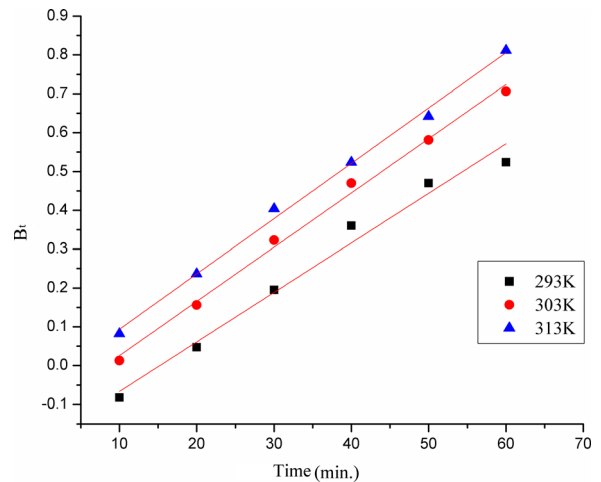

Fig. 5 Bt vs. time plot at different temperatures

evaluated from D_i, the effective diffusion coefficient (Rudzinski and Panczyk 2002; Sarkar et al. 2006b), as

$$\mathrm{FF} = q_t/q_0 \tag{19}$$

$$= 1-6/\pi^2 \cdot e^{-Bt} \tag{20}$$

$$Bt = -0.4977-\ln(1-F) \tag{21}$$

$$B = \pi^2 D_i/r^2 \tag{22}$$

where q_0 is the initial amount of fluoride (mg g^{-1}), Bt is the mathematical function of FF (the fraction of fluoride adsorbed at time t), r is the radius of adsorbent particle, and D_i is the effective diffusion coefficient.

The value of Bt calculated from each value of FF is plotted against time (Reichenberg 1953). A linearity test of the plots corresponding to three different temperatures (Fig. 5) is employed to distinguish between surface and pore diffusion-controlled rates of adsorption. It is seen that the plots are linear but do not pass through the origin, indicating that surface diffusion mainly governs

Table 7 Evaluation of transport and diffusion parameters

Temp (K)	$\beta\,10^7$ (cm s^{-1})	D_i (s cm^{-2})	$(E^{\#})$ (kJ mol^{-1})	R^2
293	1.87	4.32	16.74	0.965
303	2.03	5.83		
313	2.19	6.69		
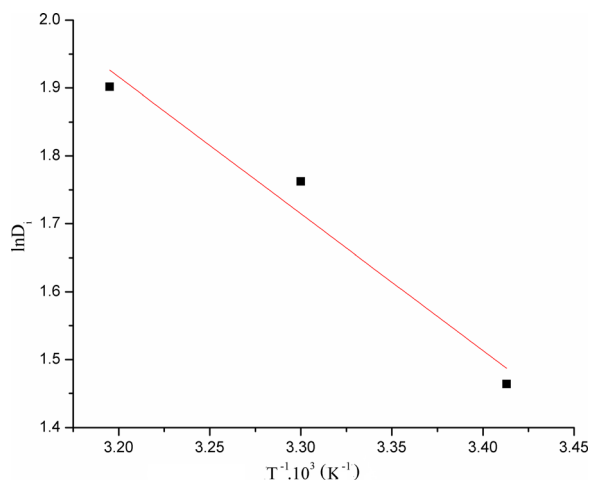
Fig. 6 $\ln D_i$ vs. T^{-1} plot

the rate-limiting process (Boyd et al. 1947) in the studied solute concentration range.

The calculated value of D_i (>4) further indicates that surface adherence dominates over particle diffusion in the present situation (Sarkar et al. 2003). However, the value of D_i is found to increase with temperature (Table 7). This is probably due to difference in mobility/retarding force on the solute particle with rise in temperature. Calculation of the activation energy ($E^{\#}$) for overall adsorption process (Gupta et al. 1997) was made via the Arrhenius equation (Eq. 23) in the form

$$\ln D_i = \ln D_0 - E^{\#}/RT \qquad (23)$$

where D_0 is the pre-exponential factor analogous to the Arrhenius frequency factor. A plot of $\ln D_i$ against T^{-1} indicates a straight line (Fig. 6). The activation energy is estimated from the slope of the regression line (R^2= 0.964) plot and is found to be 16.74 kJ mol^{-1} for an initial fluoride concentration 10 mg L^{-1}.

It seems interesting to examine the nature of interaction between fluoride and the surface of CCNB. Of the two kinds of surface interactions, i.e., physisorption and ion exchange, the later proceeds with liberation of equivalent amount of anion due to fluoride interaction.

It is found that solution pH plays an important role in determining adsorption potential of CCNB (Santra et al. 2014). The fluoride adsorption increases with increase in initial pH from 1.5 to 3.0 and decreases with increase of initial pH from 3 to 12. Maximum adsorption occurs at pH 3.0 and beyond pH 12, virtually no adsorption was observed. The decrease in fluoride uptake at high pH may be attributed to the competition of hydroxyl ions for the adsorption sites. Such an assumption is verified by measuring the final pH of the solution corresponding to each initial pH. It is found that final pH value increases largely in acidic range while negligible change is observed in alkaline solution. The fluoride interaction may thus be illustrated by Scheme 1 suggesting an ion exchange mechanism.

The presence of Ce is evidenced from the EDS and Ce–O linkage due to Ce (metal)–oxygen vibration from FTIR study. The presence of a new peak in EDS and significant shifting and intensity change of the band from 535 to 499 cm^{-1} in FTIR of fluoride-loaded CCNB clearly indicate Ce–F interaction in the adsorbent.
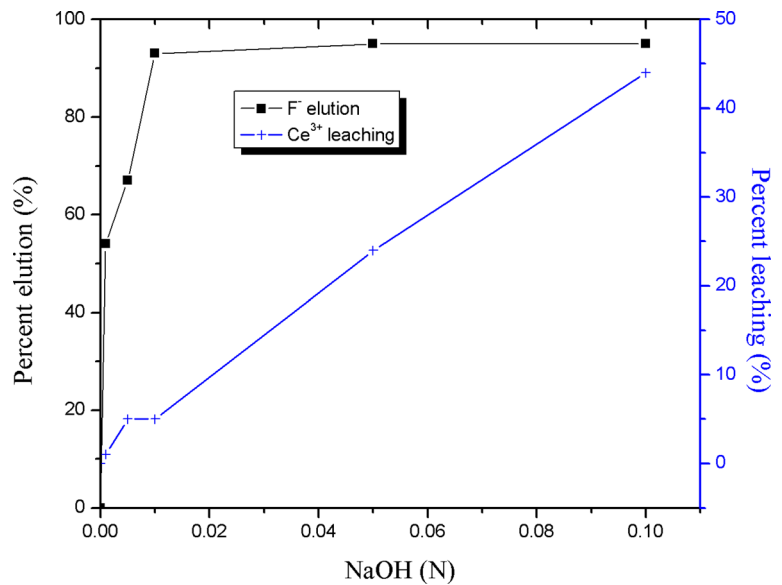
3.6 Regeneration and Reuse of CCNB

Effective elution of adsorbed fluoride from CCNB is very important for the regeneration of adsorbent via desorption. Fluoride is found to be effectively adsorbed on CCNB in the acidic pH range without any leaching of cerium and is poorly adsorbed at alkaline pH. This may provide a clue that alkaline solution can be used as the eluant. Aqueous NaOH solution of varying strength ranging from 10^{-3} to 10^{-1} N was tested for fluoride elution. It is evident from Fig. 7 that with increase of alkali strength, elution increases reach maxima (95 %) at 10^{-2} N NaOH and remains almost constant thereafter. Therefore, the regeneration of the exhausted CCNB may be done with NaOH [10^{-2} (N) or of higher strength]. At the same time, it is essential to study the stability of CCNB in terms of cerium leaching during elution. Although an insignificant leaching of cerium occurs with lower strength of NaOH (<10^{-3} N), the extent of leaching increases as the eluting strength of NaOH increases (Fig. 7).

In practical applications particularly for improving the process economics, recycling/reuse via the
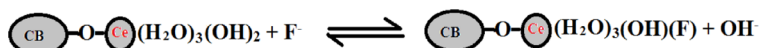
**Scheme 1** Tentative mechanism of fluoride interaction

Fig. 7 Elution and stability pattern plot

regeneration of exhausted adsorbent is a crucial factor. In order to study the possibility of reuse of CCNB, adsorption–desorption cycle was repeated. The study was conducted for elution with NaOH in the concentration range from 10^{-2} to 10^{-1} N, and the percent adsorption of fluoride on CCNB after successive adsorption–elution was investigated (Fig. 8). After five successive operations, fluoride adsorption percent decreases sharply from 94 to 17 % for higher strength of alkali (10^{-1} N) while a slow decrease in adsorption percent from 94 to 82 % is observed using 10^{-2} N alkali as eluant. This is probably due to the leaching-induced instability of CCNB. Therefore, 10^{-2} N alkali is the suitable eluant, considering the fact of minimum cerium leaching and

adequate fluoride adsorption even after recycling. The process can be recycled, at least, for five successive operations.

4 Conclusion

In an objective to optimize and model the fluoride adsorption on a novel adsorbent, the cerium-impregnated cellulose bead, statistically validated experimental design is described in the present study. The bead is analyzed for particle and surface characteristics. Presence of fluoride in the bead after adsorption is indicated in the EDS and FTIR study. The response surface methodology based on five variables was applied to categorize the significance of the variables in terms of their influence on fluoride adsorption. The central composite design was used to determine the effect of experimental variables, viz. pH (2–12), initial feed concentration (1–10 mg L^{-1}), adsorbent dose (0.1–1.5 g L^{-1}), temperature (293–323 K), and contact time (5–90 min) on fluoride adsorption. Process optimization yielding the experimental results of fluoride adsorption on CCNB agrees satisfactorily with that predicted from the model design. At the optimized condition of pH, dose, and temperature, 94 % fluoride adsorption was observed in 60 min, quite within a short treatment time compared to that reported previously. Three different isotherms were tested to find the preferred isotherm for
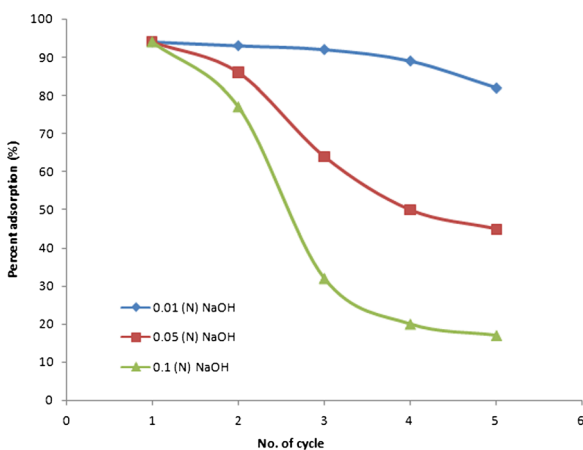
Fig. 8 Recycling of CCNB plot

fluoride adsorption on CCNB. The experimental data is fitted most to the Tempkin isotherm equation rather than Langmuir and Freundlich. The isotherm constants for each isotherm at three different temperatures were determined. The feasibility of adsorption was evaluated from the separation factor value. The adsorption kinetics follows second-order kinetic equation. Quantitative treatment of the data reveals that the surface diffusion governs the overall rate of adsorption. The activation energy using diffusion coefficient values at different temperatures was evaluated from Arrhenius equation. The tentative mechanism for fluoride interaction with CCNB (ion exchange) is predicted. The elution of fluoride is effected with NaOH (10^{-2} N) and CCNB can be reused for five successive operations.

References

Abi-aad, E., Bechara, R., Grimblot, J., & Aboukais, A. (1993). Preparation and characterization of CeO_2 under an oxidizing atmosphere. Thermal analysis XPS and EPR Study. *Chemistry of Materials, 5*(6), 793–797.

Aksu, Z., & Gonen, F. (2006). Binary biosorption of phenol and chromium (VI) onto immobilized activated sludge in a packed bed: prediction of kinetic parameters and breakthrough curves. *Separation and Purification Technology, 49*(3), 205–216.

Alagumuthu, G., & Ranjan, M. (2010). Kinetic and equilibrium studies on fluoride removal by zirconium (IV) impregnated ground nut shell carbon. *Hemijska Industrija, 64*(4), 295–304.

Allen, S. J., Mckay, G., & Porter, J. F. (2004). Adsorption isotherm models for basic dye adsorption by peat in single and binary component systems. *Journal of Colloid Interface Science., 280*, 322–333.

Behbahani, M., Moghaddam, M. R. A., & Arami, M. (2011). Techno-economical evaluation of fluoride removal by electrocoagulation process: optimization through response surface methodology. *Desalination, 271*(1/3), 209–218.

Boyd, G. E., Adamson, L. S., & Meyers, L. S. (1947). The exchange adsorption of ions from aqueous solution by organic zeolites; kinetics. *Journal of the American Chemical Society, 69*(11), 2836–2848.

Brereton, R. G. (2003). *Chemometrics: data analysis for the laboratory and chemical plant*. West Sussex: Wiley.

Camacho, L. M., Torres, A., Saha, D., & Deng, S. (2010). Adsorption equilibrium and kinetics of fluoride on sol-gel-derived activated alumina adsorbents. *Journal of Colloid and Interface Science, 349*(1), 307–313.

Castel, C., Schweizer, M., Simonnot, M. O., & Sardin, M. (2000). Selective removal of fluoride ions by a two-way ion-exchange cyclic process. *Chemical Engineering Science, 55*(17), 3341–3352.

Chand, D. (1999). Fluoride and human health—causes for concern. *Indian Journal of Environmental Protection, 19*(2), 81–89.

Chiou, M. S., & Li, H. Y. (2003). Adsorption behavior of reactive dye in aqueous solution on chemical cross-linked chitosan beads. *Chemosphere, 50*(8), 1095–1105.

Crank, J. (1956). *The mathematics of diffusion*. Oxford: Clarendon.

Freundlich, H. M. F. (1906). Over the adsorption in solution. *Journal of Physical Chemistry, 57*(1906), 385–471.

Ghiaci, M., Abbaspur, A., Kia, R., & Seyedeyn-Azad, F. (2004). Equilibrium isotherm studies for the sorption of benzene, toluene, and phenol onto organo-zeolites and as-synthesized MCM-41. *Separation and Purification Technology, 40*(3), 217–229.

Goksungur, Y., Uren, S., & Guvenc, U. (2005). Biosorption of cadmium and lead ions by ethanol treated waste baker's yeast biomass. *Bioresource Technology, 96*(1), 103–109.

Gupta, V. K., Sriastava, S. K., & Mohan, D. (1997). Equilibrium uptake, sorption dynamics, process optimization and column operation for the removal and recovery of malachite green from wastewater using activated carbon and activated slag. *Industrial and Engineering Chemistry Research, 36*(6), 2207–2218.

Ho, Y. S., & McKay, G. (1999). Pseudo-second-order model for sorption processes. *Process Biochemistry, 34*(5), 451–465.

Hu, C. Y., Lo, S. L., & Kuan, W. H. (2005). Effects of the molar ratio of hydroxide and fluoride to Al(III) on fluoride removal by coagulation and electro coagulation. *Journal of Colloid and Interface Science, 283*(2), 472–476.

Jagtap, S., Thakre, D., Wanjari, S., Kamble, S., Labhsetwar, N., & Rayalu, S. (2009). New modified chitosan-based adsorbent for defluoridation of water. *Journal of Colloid and Interface Science, 332*(2), 280–290.

Jagtap, S., Yenkie, M. K., Labhsetwar, N., & Rayalu, S. (2012). Fluoride in drinking water and defluoridation of water. *Chemical Review, 112*(4), 2454–2466.

Langmuir, I. (1916). The constitution and fundamental properties of solids and liquids. *Journal of American Chemical Society, 38*(11), 2221–2295.

Larsen, M. J., & Pearce, E. I. F. (2002). Defluoridation of drinking water by boiling with brushite and calcite. *Caries Research, 36*(5), 341–346.

Li, Z., Deng, S., Zhang, X., Zhou, W., Huang, J., & YU, G. (2010). Removal of fluoride from water using titanium-based adsorbents. *Frontiers of Environmental Science & Engineering in China, 4*(4), 414–420.

Mckay, G., Allen, J. S., McConvey, I. F., & Otterbeurn, M. S. (1981). Transport process in the sorption of ions by peat particles. *Journal of Colloid and Interface Science, 80*(2), 323–339.

Medellin-Castillo, N. A., Leyva-Ramos, R., Ocampo-Perez, R., Garcia de la Cruz, R. F., Aragon-Pina, A., Martinez-Rosales,

J. M., Guerrero-Coronado, R. M., & Fuentes-Rubio, L. (2007). Adsorption of fluoride from water solution on bone char. *Industrial & Engineering Chemistry Research, 46*(26), 9205–9212.

Montgomery, D. C. (2009). *Design and analysis of experiments* (7th ed.). Hoboken: Wiley.

Reichenberg, D. (1953). Properties of ion exchange resins in relation to their structures. III. Kinetics of exchange. *Journal of the American Chemical Society, 75*(3), 589–597.

Rengaraj, S. J., Yeon, W., Kim, Y., Jung, Y., Ha, Y. K., & Kim, W. H. (2007). Adsorption characteristics of Cu(II) onto ion exchange resins 252H and 1500H: kinetics, isotherms and error analysis. *Journal of Hazardous Materials, 143*(1/2), 469–477.

Rocha, R. A., & Muccillo, E. N. S. (2003). Physical and chemical properties of nanosized powders of gadolinia-doped ceria prepared by the cation complexation technique. *Materials Research Bulletin, 38*(15), 1979–1986.

Rudzinski, W., & Panczyk, T. (2002). Remarks on the current state of adsorption kinetic theories for heterogeneous solid surfaces: a comparison of the ART and the SRT approaches. *Langmuir, 18*(2), 439–449.

Santra, D., Joarder, R., & Sarkar, M. (2014). Taguchi design and equilibrium modeling for fluoride adsorption on cerium loaded cellulose nanocomposite bead. *Carbohydrate Polymers, 111*, 813–821.

Sarici-Özdemir, Ç., & Önal, Y. (2014). Error analysis studies of dye adsorption onto activated carbon from aqueous solutions. *Particulate Science and Technology, 32*(1), 20–27.

Sarkar, M., & Majumdar, P. (2011). Application of response surface methodology for optimization of heavy metal biosorption using surfactant modified chitosan bead. *Chemical Engineering Journal, 175*, 376–387.

Sarkar, M., Acharya, P., & Bhattacharya, B. (2003). Modeling the adsorption kinetics of some priority organic pollutants in water from diffusion and activation energy parameters. *Journal of Colloid and Interface Science, 266*(1), 28–32.

Sarkar, M., Banerjee, A., & Pramanick, P. P. (2006a). Kinetics and mechanism of fluoride removal using laterite. *Industrial and Engineering Chemistry Research, 45*(17), 5920–5927.

Sarkar, M., Banerjee, A., Pramanik, P. P., & Sarkar, A. R. (2006b). Use of laterite for the removal of fluoride from contaminated drinking water. *Journal of Colloid and Interface Science, 302*(2), 432–441.

Sarkar, M., Manna, S., & Pramanik, P. P. (2008). Evaluation of the efficiency of fly ash from thermal power plant in controlling aquatic pollution. *Journal of Indian Chemical Society, 85*(11), 1130–1133.

Sehn, P. (2008). Fluoride removal with extra low energy reverse osmosis membranes: three years of large scale field experience in Finland. *Desalination, 223*(1/3), 73–84.

Sereshti, H., Karimi, M., & Samadi, S. (2009). Application of response surface method for optimization of dispersive liquid-liquid microextraction of water-soluble components of Rosa damascena Mill. essential oil. *Journal of Chromatography A, 1216*(2), 198–204.

Temkin, M. I., & Pyzhev, V. (1940). Kinetics of ammonia synthesis on promoted iron catalysts. *Acta Physiochimica URSS, 12*(3), 217–222.

Teutli-Sequeira, A., Solache-Ríos, M., & Balderas-Hernández, P. (2012). Modification effects of hematite with aluminum hydroxide on the removal of fluoride ions from water. *Water, Air, and Soil Pollution, 223*(1), 319–327.

Veressinina, Y., Trapido, M., Ahelik, V., & Munter, R. (2001). Proceedings of the Estonian Academy of Sciences. Chemistry, 50*(2), 81–88.

Viswanathan, N., Sundaram, C. S., & Meenakshi, S. (2009). Removal of fluoride from aqueous solution using protonated chitosan beads. *Journal of Hazardous Materials, 161*(1), 423–430.

Wang, D. M., Hao, G., Shi, Q. H., & Sun, Y. (2007). Fabrication and characterization of superporous cellulose bead for high-speed protein chromatography. *Journal of Chromatography A, 1146*(1), 32–40.

Weber, T. W., & Chakravorti, R. K. (1974). Pore and solid diffusion models for fixed-bed adsorbers. *American Institute of Chemical Engineers Journal, 20*(2), 228–238.

Yadav, A. K., Abbassi, R., Gupta, A., & Dadashzadeh, M. (2013). Removal of fluoride from aqueous solution and groundwater by wheat straw, sawdust and activated bagasse carbon of sugarcane. *Ecological Engineering, 52*, 211–218.